NASA Contractor Report 198325

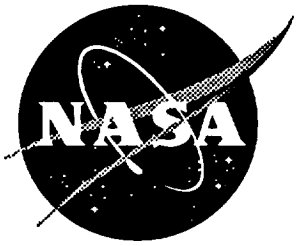

Planetary Boundary Layer Simulation Using TASS

David G. Schowalter, David S. DeCroix, Yuh-Lang Lin, S. Pal Arya, and Michael Kaplan
North Carolina State University, Raleigh, North Carolina

Cooperative Agreement NCC1-188

April 1996

National Aeronautics and
Space Administration
Langley Research Center
Hampton, Virginia 23681-0001

Abstract

Boundary conditions to an existing large-eddy simulation model have been changed in order to simulate turbulence in the atmospheric boundary layer. Several options are now available, including the use of a surface energy balance. In addition, we compare convective boundary layer simulations with the Wangara and Minnesota field experiments as well as with other model results. We find excellent agreement of modelled mean profiles of wind and temperature with observations and good agreement for velocity variances. Neutral boundary layer simulation results are compared with theory and with previously used models. Agreement with theory is reasonable, while agreement with previous models is excellent.

TABLE OF CONTENTS

Section Page

LIST OF TABLES

LIST OF FIGURES

Figure 9. (a) Horizontal and (b) vertical velocity variances for the Minnesota Experiment, Run 5A1.

Figure 10. Vertical heat flux for Run 5A1 of the Minnesota Experiment.

Figure 11. Dimensionless wind shear profiles for a neutral boundary layer from (*a*) TASS and (*b*) Andren *et al.* (1994).

Figure 12. Same as figure 11 but for Φ_c.

1. Introduction

Over the past two years, this group has been working in support of the numerical modeling arm of the NASA Wake Vortex Program. It is believed that the turbulence in the planetary boundary layer will have a significant effect on the evolution of wake vortices. Therefore, a first step is the accurate simulation of this turbulence using Large-eddy simulation. Eventually, a nested grid capability will enable the insertion of a wake vortex pair into the boundary layer. Our goal has been to add proper boundary conditions and to validate the TASS (Terminal Area Simulation System) model for the planetary boundary layer simulation.

What follows in Section 2 is a description of the boundary condition changes to TASS and the associated theory. Section 3 discusses the validation results and Section 4 contains a discussion of neutral boundary layer runs. Section 5 is a summary and we have also included an appendix with instructions for using the boundary layer options with the model.

2. New boundary conditions in TASS

The horizontal velocity at the top of the computational domain may now be specified. This is accomplished with a three layer sponge technique much like what was done previously with potential temperature. This velocity may be a function of time.

The geostrophic wind may now be specified. It is not a function of time, but may be a function of height. This is equivalent to specification of the horizontal pressure gradient.

There is a choice of four possible heating (cooling) boundary conditions at the bottom of the computational domain:

1. Simple uniform heating specified as a function of time in which a rate term (in W/m^2) is added to the equation for potential temperature at the ground. This should not be used for large heating rates because strong temperature gradients will not be properly accounted for in the surface layer similarity scheme.

2. Specification of surface heat and moisture fluxes in kinematic units (°K·m/s and m/s). In this case, the rate terms are added to the equations for potential temperature and for water vapor at the ground. In addition, the Obukhov length is properly calculated using the value of the heat flux rather than using temperature gradients which may be under-resolved.

3. Specification of the air temperature and moisture close to the ground. Surface layer similarity is then used to calculate the proper heat and moisture fluxes. Again, the Obukhov length is calculated using the surface heat flux. This method was described in detail in our recent Annual Report (Lin *et al.* 1994).

4. Use of a surface energy budget for calculation of soil moisture, soil temperature, and the resulting heat and moisture fluxes to the atmosphere. We use the slab model introduced by Bhumralkar (1975) and Blackadar (1976).

The details and validation of method 4 have not been shown previously and will be given here. In addition, we will discuss validation results for the simulation of the Atmospheric Boundary Layer in general.

2.1 Surface Energy Budget: Theory

The surface energy budget is essentially equivalent to the one proposed by Bhumralkar (1975) and Blackadar (1976). This method was tested by Deardorff (1978) and shown to be both efficient and accurate. Although this addition was a central item on our original proposal, it was felt that the code should be as simple as possible. The first reason for this is that the option will be used rarely. The original plans for our research did not include either of the other surface boundary condition options, which are simpler *and* more accurate than a surface energy balance. To clarify, the purpose of the entire surface energy balance scheme is to calculate the surface heat and moisture fluxes. A large number of parameters describing soil characteristics goes into the scheme. Many of these are usually not known accurately if they are known at all. If, however, the surface heat and moisture flux are known with any degree of accuracy, it makes infinitely more sense to use those values than to try to predict them using parameters that are questionable. The same is true if the temperature and humidity are known at some level close to the ground. The second reason for keeping the scheme simple is to minimize the additional computational time during its use. For these reasons, a vegetation layer has not been included in the surface energy budget code.

The scheme models the soil as a thin slab whose temperature changes throughout the day above a substrate whose temperature remains constant. The rate equation for the temperature of the slab can then be written as

$$\frac{\partial T_s}{\partial t} = -c_1(Q_h + L_h E_g - Q_r)/(\rho_s c_s d_1) - c_2(T_s - T_m)/\tau_1$$

where T_s is the slab temperature, T_m is the temperature of the substrate, c_s is the heat capacity of the soil, τ_1 is the diurnal period, ρ_s is the density of the soil, d_1 is the depth of the slab, Q_h is the sensible heat flux to the atmosphere, Q_r is the net radiative heat flux to the slab, E_g is the rate of evaporation of soil moisture, and L_h is the latent heat of evaporation. c_1 and c_2 are constants, set to $2\pi^{1/2}$ and 2π respectively. The last term represents the heat exchanged between the slab and the substrate. We may write

$$d_1 = \sqrt{\lambda_s \tau_1},$$

where λ_s is the thermal conductivity of the soil.

The radiative heat flux may be written as

$$Q_r = K_s + I\downarrow - I\uparrow,$$

where K_s represents the solar radiation, $I\downarrow$ the incoming longwave radiation, and $I\uparrow$ the outgoing longwave radiation. The outward radiative flux is straightforwardly written as

$$I\uparrow = \varepsilon_g \sigma T_s^4,$$

ε_g being the emmisivity of the ground and σ being the Stefan-Boltzmann constant. The incoming longwave radiation is more complicated and must be parameterized. Like Deardorff, we use the approximation of Staley and Jurica (1972),

$$I\downarrow = \{\sigma_l + \sigma_m + \sigma_h + [1-(\sigma_l + \sigma_m + \sigma_h)][0.67][1670 q_a]^{0.08}\}\sigma T_a^4,$$

in which q_a is the mean humidity at the first model level in the atmosphere and σ_l, σ_m, and σ_h are the cloud fractions for middle, low, and high clouds, respectively. Incoming solar radiation is written as

$$K_s = (1370\frac{\mathrm{W}}{\mathrm{m}^2})T_K(1-\alpha)\sin\Psi$$

in which α represents the albedo of the ground, T_k is the transmissivity of the atmosphere, and Ψ is the solar zenith angle. Following Stull (1988),

$$T_K = (0.6 + 0.2\sin\Psi)(1-0.4\sigma_h)(1-0.7\sigma_m)(1-0.4\sigma_l)$$

and

$$\sin\Psi = \sin\phi\sin\delta_s - \cos\phi\cos\delta_s\cos[(\frac{\pi t_{UTC}}{12}) - \lambda_E],$$

where δ_s is the solar declination angle, ϕ is the latitude in radians, λ_e is the longitude in radians, and t_{utc} is the time at 0° longitude. We may write the solar declination angle as

$$\delta_s = \phi_r\cos[\frac{2\pi(d-d_r)}{365.25}],$$

where d is the day number (out of 365) and d_T (173) is the day of the summer solstice.

Q_h, the sensible heat flux is estimated as

$$Q_h = \rho c_p u_* \theta_*,$$

where

$$u_* = \frac{k\sqrt{u^2 + v^2}}{\ln(\frac{z}{z_0}) - \Psi_M(\frac{z}{L})},$$

and

$$\theta_* = \frac{k(\theta - \theta_0)}{\ln(\frac{z}{z_0}) - \Psi_H(\frac{z}{L})}.$$

In these equations, z_0 is the surface roughness length, z the height above the ground, u the mean eastward horizontal velocity, v the mean northward horizontal velocity, θ the potential temperature, θ_o the potential temperature at z_0, and L the Obukhov length. The functional forms used for $\Psi_M(z/L)$ and $\Psi_H(z/L)$ are given in Lin *et al.* (1994). The problem which then arises is to calculate θ_0. We use the formula of Zilitinkevich (1970),

$$\theta_0 = \theta_s + \frac{0.74}{k}\theta_*[0.13(\frac{u_* z_0}{\nu})^{0.45}],$$

in which ν is the kinematic viscosity of air, θ_s is the potential temperature of the surface (slab), and u_* and θ_* from the previous time step are used.

Moisture flux, E_g, is calculated in the same manner. We let

$$E_g = \rho u_* q_*,$$

where

$$q_* = \frac{k(q - q_0)}{\ln(\frac{z}{z_0}) - \Psi_H(\frac{z}{L})},$$

$$q_0 = q_s + \frac{0.74}{k} q_* [0.13(\frac{u_* z_0}{\nu})^{0.45}],$$

and q represents the moisture fraction (g/g) in the atmosphere.

We now come to the determination of the surface value of the moisture fraction. Following Deardorff (1978), a slab model is used for moisture as well as temperature. Thus, we let w_g denote the soil moisture fraction in uppermost portion and $w2$ represent this value for the substrate. q_S, the surface atmospheric moisture fraction is given as

$$q_s = \alpha' q_{sat}(T_s, P_s) + (1 - \alpha') q_a \qquad q_s \le q_{sat}(T_s, P_s)$$

$$\alpha' = \min(1, w_g / w_k),$$

where w_k is the value of w_g at which the atmosphere is saturated and $q_{sat}(T_s,P_s)$ is the atmospheric saturation mixing ratio at the surface. The rate equation for the slab soil moisture is

$$\frac{\partial w_g}{\partial t} = -C_1 \frac{(E_g - P)}{\rho_w d_1'} - C_2 \frac{(w_g - w_2)}{\tau_1} \qquad 0 \le w_g \le w_{max},$$

where , ρ_w is the density of liquid water, P is the horizontally meaned precipitation rate. w_{max} is the maximum value of w_g above which runoff occurs. We let d_1' be 10 cm and d_2' be 50 cm, typical values for most soils. We let C_2 be 0.9. C_1 depends upon soil moisture in the following way:

$$C_1 = 0.5 \qquad w_g / w_{max} \ge 0.75$$

$$C_1 = 14 - 22.5[(w_g/w_{max})-0.15] \qquad 0.15 \le w_g / w_{max} \le 0.75$$

$$C_1 = 14 \qquad w_g / w_{max} \le 0.15$$

The rate equation for w_2 is

$$\frac{\partial w_2}{\partial t} = \frac{-(E_g - P)}{\rho_w d_2'} \qquad 0 \le w_2 \le w_{max}$$

3. Validation

3.1 Surface energy budget validation

The energy budget scheme was tested as a self-standing entity (outside of TASS) with data from Day 1 in Lettau & Davidson (1957). This extensive field experiment was performed near O'Neill, Nebraska. The ground and radiative heat fluxes were measured directly and the latent and sensible heat fluxes could be estimated by assuming surface layer similarity and using the given vertical profiles of temperature and humidity. For the atmospheric wind speed as a function of time, we linearly interpolated between the values given in Lettau & Davidson, table 4.2 at a height of 6.4 m starting at 0035 local time. The atmospheric humidity (mixing ratio) was converted from the vapor pressure values given in their table 4.3.a. The linear interpolation was done in the same manner. Wind speed at the same height was taken from table 4.1.a and interpolated. Thus these values which are normally contained at the first grid level within TASS were taken from observed data for this validation.

The soil moisture variables were assigned in the following way. Moisture tension values given in table 2.3 of Lettau & Davidson were used in conjunction with soil temperatures in table 2.1.a and the graph (figure 2.3.3, p. 54) to estimate the mass ratio of water to soil. To calculate the volume ratio, we then use

$$w = \frac{\rho_s r_m}{\rho_w},$$

where r_m is the mass ratio, ρ_s is the density of the dry soil (shown in figure 2.2.3.2), and ρ_w is the density of liquid water. We estimated values of soil moisture for 5 cm. depth (slab), and 40 cm. depth (substrate). The next difficulty is estimating w_k. The soil at O'Neill, Nebraska for the referenced study was described as a "sandy loam." In Sellers

(1965), we see that for dry clay soil, the volume ratio of solid to total is 0.417. For sand, the ratio is 0.585. Thus, one would estimate that for a sandy loam, the correct ratio might be roughly 0.5. For a sandy loam, Sellers lists the field capacity to be 0.43 times this ratio. The field capacity is the maximum amount of water that a soil can hold against gravity. Thus we have a volume of 0.22 for the field capacity. One would guess that the moisture fraction at which the *air* at the ground is saturated would be somewhat larger than the field capacity. Thus, we use w_k=0.30. A summary of all soil parameters is shown table 1 of this paper.

α	0.25
λ_S (m^2/s)	0.5×10^{-6}
$\rho_S c_S$ (j/m^3K)	1.51×10^{-6}
ε	0.90
w_2	0.21
w_g	0.16
w_k	0.30

Table 1. Soil parameters used for energy budget validation case.

Heat flux and moisture flux for the observational data were calculated from the given profiles by assuming surface layer similarity. In figure 1, these are plotted against the calculated values. Notice that, for heat flux, the observed and calculated values are nearly identical until about 0700, local time. After this time, the agreement is fair. Figure 2 shows the time history of the other portions of the energy budget. All are in good agreement with observation with the exception of the latent heat flux. This is considerably larger in magnitude than the observations in the early morning and considerably smaller than observations in the afternoon. This discrepancy is what causes the mild disagreement with the sensible heat flux. Early in the morning, the larger latent heat flux results in a smaller sensible heat flux, and vice versa in the afternoon. This is due to the lack of a

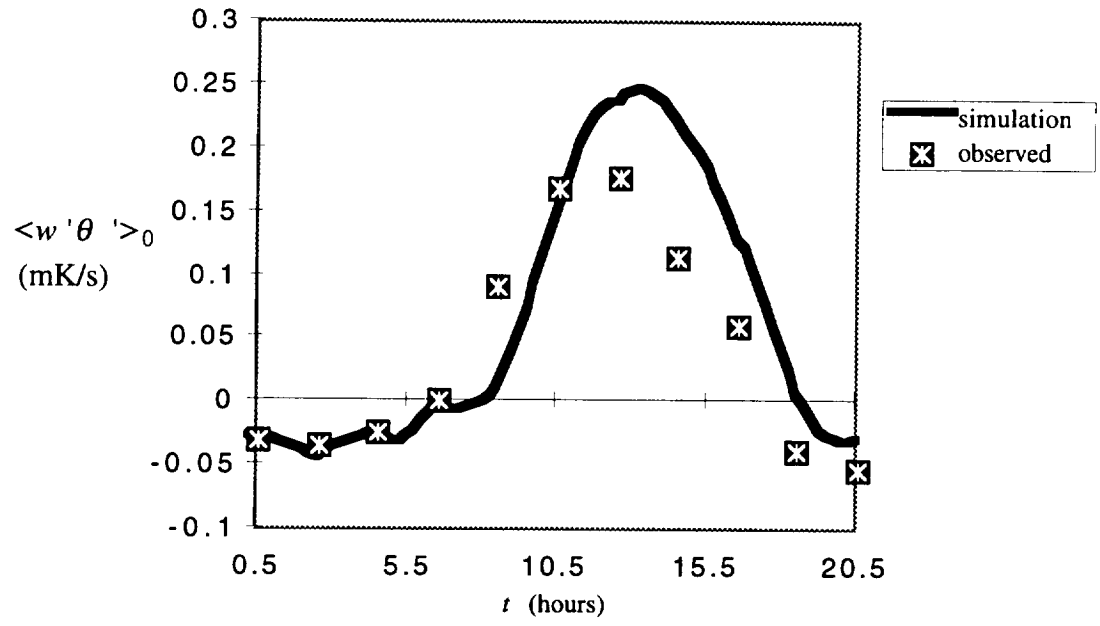

Figure 1. Sensible heat flux for the validation case compared with observed values. Observed values were calculated from observed profiles by assuming surface layer similarity.

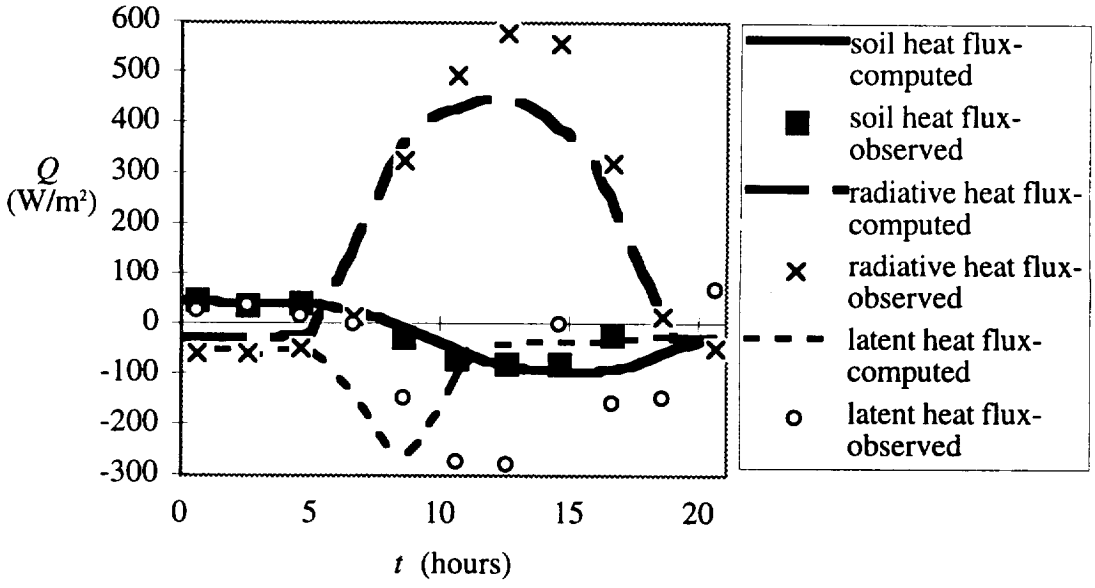

Figure 2. Radiative, latent, and soil heat flux for the validation case. Observed values were measured directly for the radiative heat fluxes, were numerically calculated in Lettau & Davidson for the soil heat flux from temperature profiles, and were deduced for the latent heat flux by assuming surface layer similarity.

vegetation parameterization in the model. Deardorff (1978) shows the same effect when comparing results with and without vegetation parameterization.

Thus, as mentioned in section 1, we have chosen an energy budget scheme which is simple and provides acceptably accurate results. If deemed necessary in the future, we may add parameterization for vegetation, which would increase the accuracy.

3.2 Wangara Validation

Validation of TASS with data from the Wangara Experiment (Clarke *et al.* 1971) has been discussed in some detail by Lin *et al.* (1994). The subgrid contribution to the velocity variances, however, were estimated incorrectly in that paper. Thus, we will show the most important results here. In this case, temperature and moisture at 2m were specified. These values were given in the data report. Resolution for the case shown is 40X40X40, with a horizontal grid resolution of 125 m. and a vertical resolution of 50 m. Figure 3 shows how well this boundary condition works for the potential temperature. Shown are the potential temperature profiles for 0900, 1200, and 1500 local time. The 0900 profile is from the observations and was used to initialize the model. Note that there is larger scatter in the observed data, because they represent single point measurements. The model output was averaged horizontally. The higher potential temperature near the surface for the 1500 observations probably indicates that the rawinsonde balloon was released within a thermal plume. The mean potential temperature within the mixed layer is constant, and the agreement at the top of the boundary layer is excellent, meaning the balloon has probably moved outside of the thermal by this time.

In figure 4, we compare the TASS results for mean winds with the observations and with Deardorff's (1974) results. Again, the scatter in the observed data is due to the single

point nature of the measurements. It is clear from the figure that TASS predicts the wind speeds extremely well.

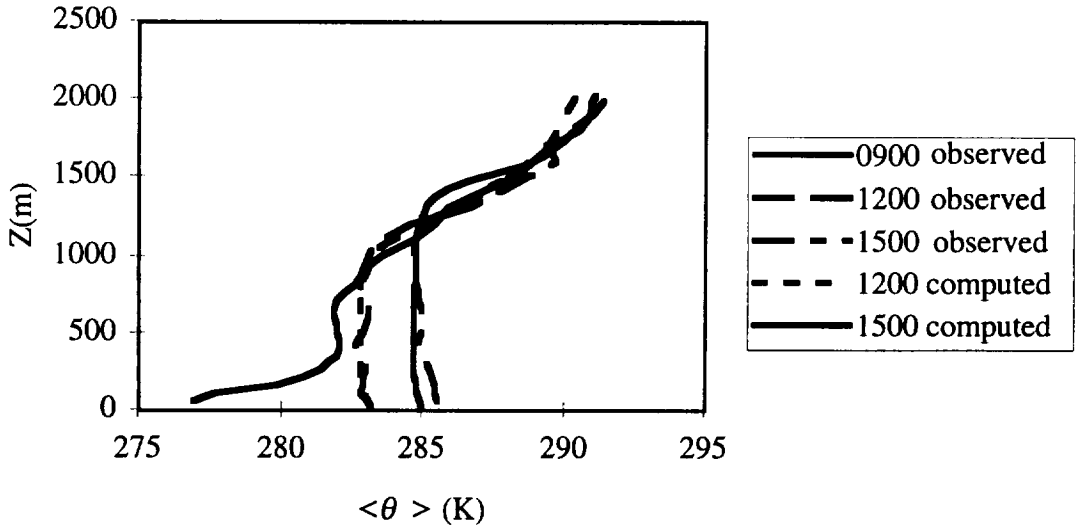

Figure 3. Observed and computed potential temperature profiles for the Wangara Experiment, Day 33. The 0900 profile was used to initialize the model.

Horizontal and vertical velocity variances are shown in figure 5. The variances are non-dimensionalized with $w*$, the velocity scale for a convective boundary layer ($w*=[g\langle w'\theta'\rangle_0 Z_i/\langle\theta\rangle]^{1/3}$). Here, Z_i is the mixed layer depth, g is the gravitational acceleration, $\langle w'\theta'\rangle_0$ is the heat flux at the surface, and $\langle\theta\rangle$ is the mean potential temperature within the mixed layer. Although no turbulence statistics were measured in the Wangara Experiment, typical dimensionless values for these variances within convective mixed layers are between 0.2 and 0.4, which agrees well with our results.

In addition, we have run one simulation of the Wangara case using the energy budget scheme. Table 2 shows the soil parameters used. Results for potential temperature are shown in figure 6. Notice that the temperature specification boundary condition

(previously shown) is much more accurate. The energy budget results, however, are just as accurate as the results of Pleim & Xiu (1995), who used a similar soil model with a one dimensional simulation of Wangara Day 33.

3.3 Minnesota Validation

Because the Wangara Experiment contained no data on turbulent intensities and fluxes, it was necessary to look elsewhere for validation of these quantities. We chose the Minnesota Experiment of 1973 (Izumi & Caughey, 1976). One of the difficulties in this case is that the large scale pressure gradients are not known. For example, as previously mentioned, the geostrophic wind profile may be used by the model. These profiles, however, were not measured in the experiment. To account for this forcing, we obtained synoptic network rawinsonde data (available every twelve hours) on the day of the experiment we chose to simulate. We then performed an objective analysis to extract geostrophic winds as a function of height within our model domain. This is extremely important for predicting mean horizontal winds and for comparing momentum fluxes with observed values. As described in Lin *et al.* (1994), for a steady flow,

$$f(\langle u\rangle - u_g) = -\frac{\partial}{\partial z}\langle v' w'\rangle$$

$$f(\langle v\rangle - v_g) = \frac{\partial}{\partial z}\langle u' w'\rangle$$

where f is the Coriolis parameter, u is the eastward velocity, v the northward velocity, w the vertical velocity, u_g and v_g denote the geostrophic components, and $\langle\rangle$ denotes averaging. The twelve hour spaced geostrophic wind data was then interpolated in time to correspond to the middle of our run, remaining constant throughout the run. The

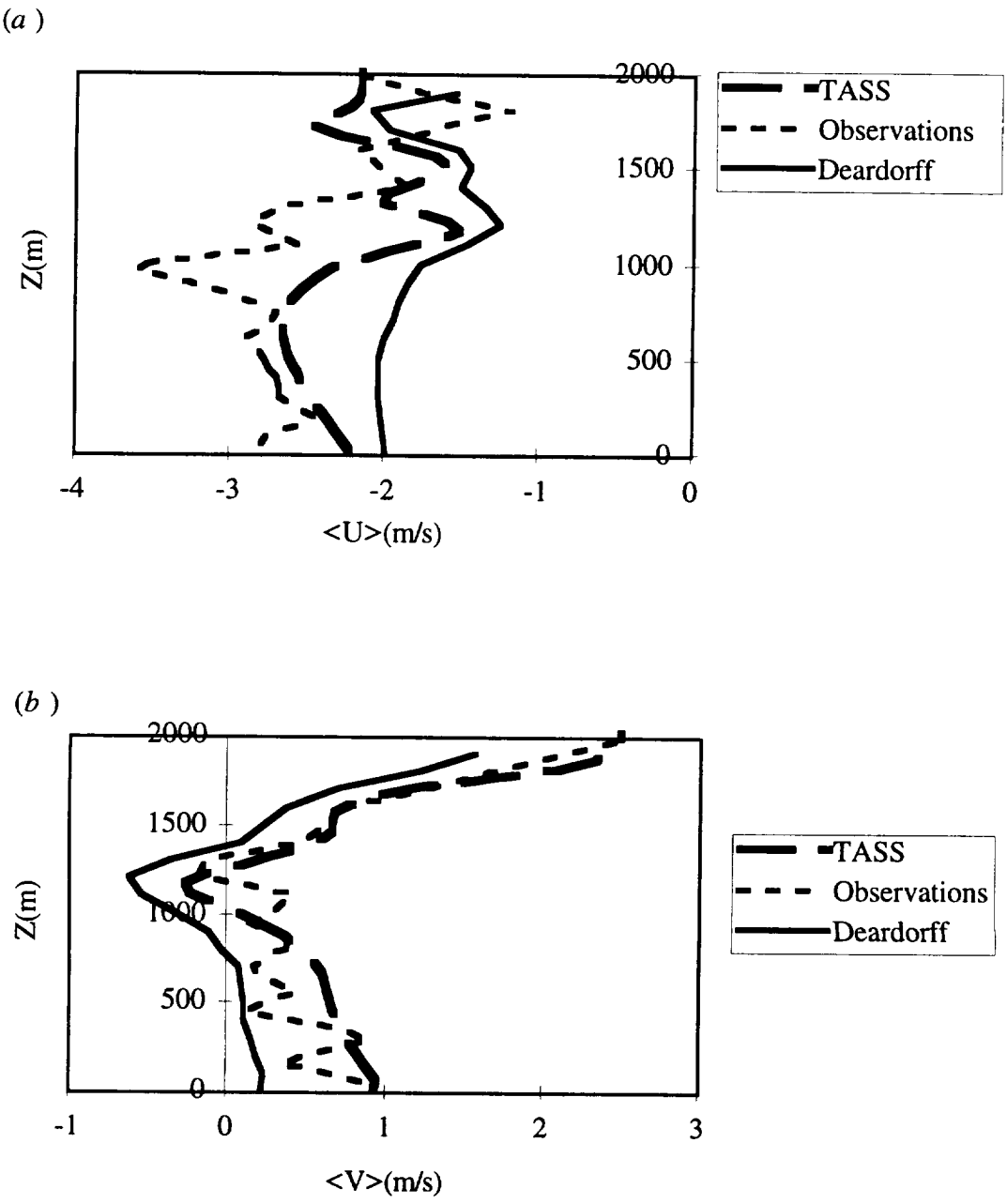

Figure 4. Comparison of mean horizontal velocity results from TASS with Deardorff (1974) and with observed data. (a) Eastward wind component and (b) northward wind component. Results shown are for 1200 local time, after three hours of simulation.

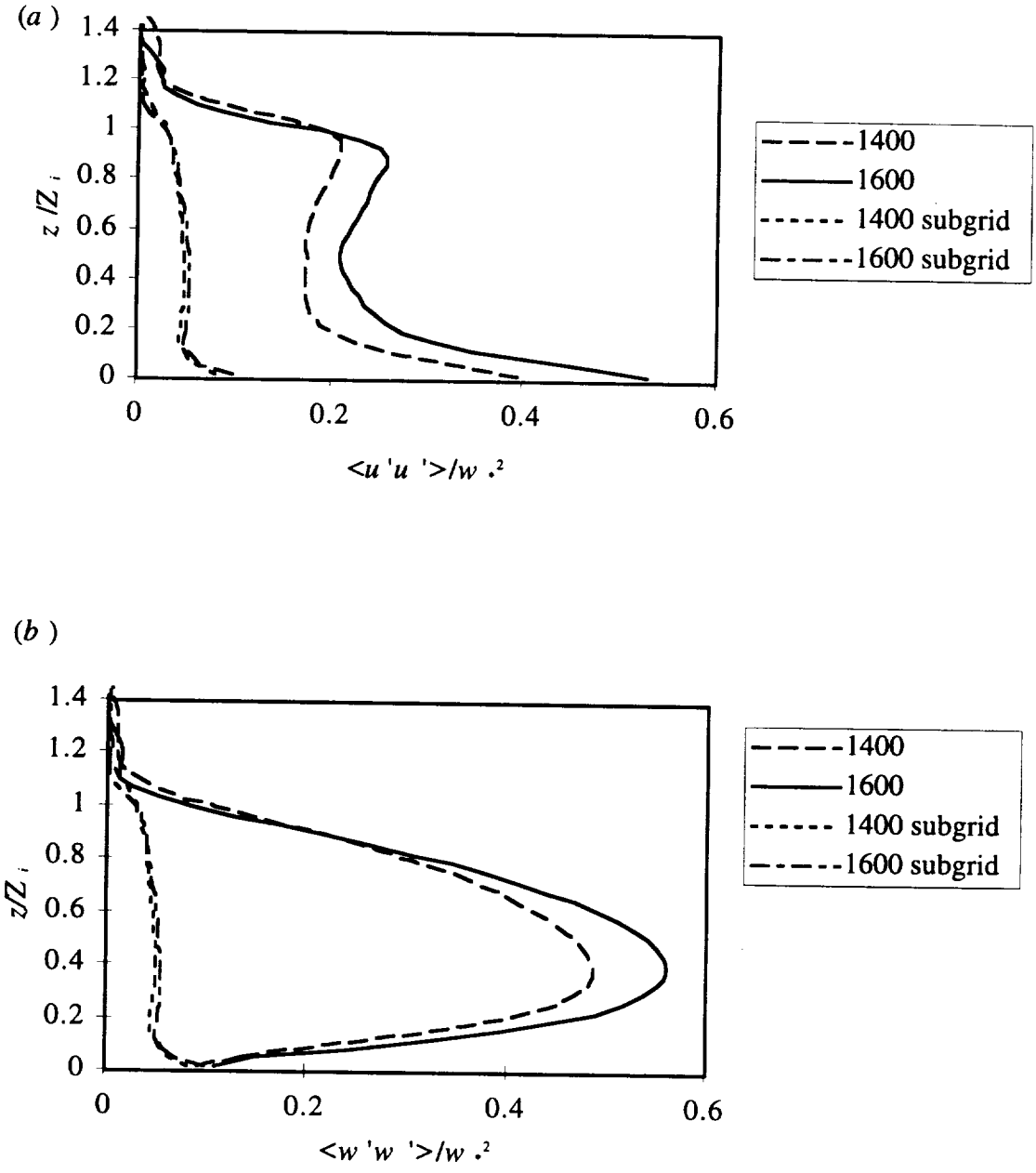

Figure 5. (a) Horizontal and (b) vertical velocity variances for the TASS simulation of the Wangara Experiment. Values were averaged horizontally over the domain as well as over one hour in time, centered on the local hour indicated. Subgrid contributions are estimates based on the magnitude of the local deformation tensor.

α	0.25
λ_S (m^2/s)	0.5 X 10^{-6}
$\rho_S c_S$ (J/m^3K)	2.1 X 10^{-6}
ε	0.85
w_2	0.0245
w_g	0.002
w_k	0.2

Table 2. Soil parameters used for the Wangara case.

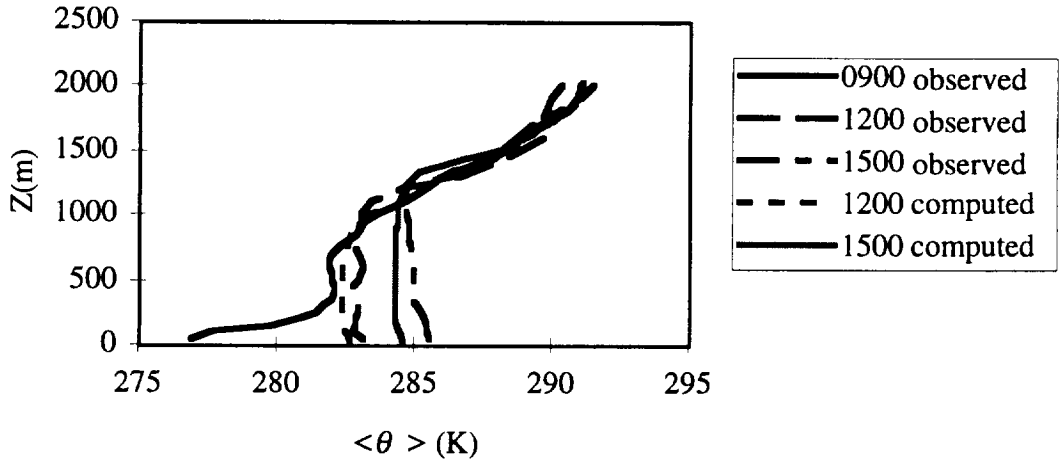

Figure 6. Observed and computed potential temperature profiles for Wangara Day 33 using the energy budget scheme in TASS. The observed 0900 profile was used to initialize the model.

model used a 70X70X50 grid, with 50 meter horizontal resolution, and 36 meter vertical resolution with periodic horizontal boundary conditions. Flux specification was used for the lower boundary heating condition.

The model was initialized with a 1259 local time sounding from the experimental site on September 15, 1973. Run 5A1, with which we are comparing, contains quantities

averaged from 1622 to 1737 local time. Thus the model is run for over three hours before the comparison. Model averaging was accomplished by averaging horizontally over the entire domain. These averages were taken every five minutes and, in turn, averaged over the 75 minutes of the experiment. The experimental mixed layer height, Z_i, was 1085 meters. The model, however, predicted a height of 1420 meters. This disparity is due primarily to an overestimate of the heat flux between 1259 and the observation period. Only the average surface heat flux during the observation period was given.

Figure 7 shows a comparison of observed and modeled average winds. The overall magnitude is in good agreement, but the observed winds show a large shear within the mixed layer. This is most probably due to a mesoscale effect which could not be captured by the geostrophic wind profiles deduced from the synoptic data. This brings us to figure 8, which shows the vertical momentum fluxes as a function of height. The flux of northward momentum, $<v'w'>$, is in excellent agreement with the observed values. The flux of eastward momentum, $<u'w'>$, is in fair agreement. The curve's shape is similar to the observed profile, but the magnitudes do not agree higher up in the mixed layer. Again, this is a mesoscale effect and the results are quite good considering the data available for our synoptic forcing.

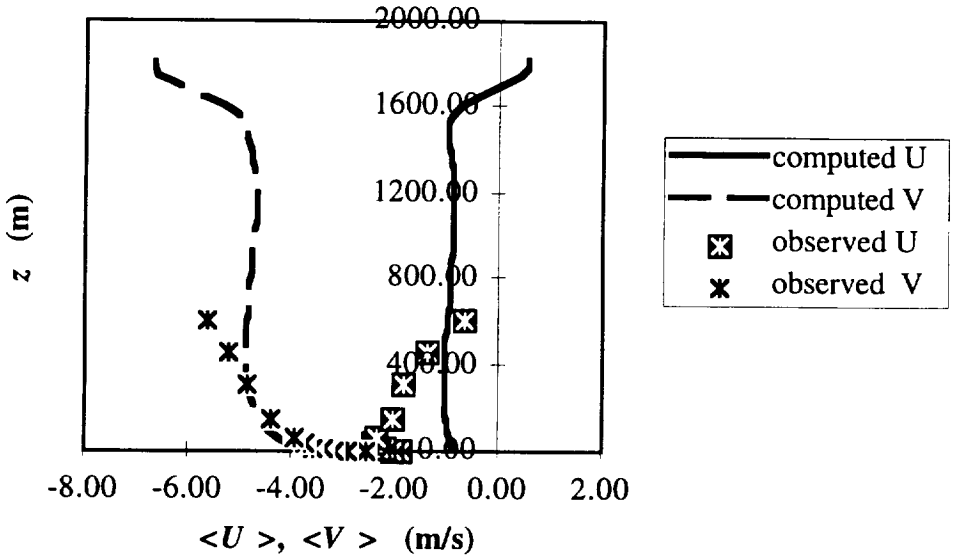

Figure 7. Comparison of computed mean winds with observed winds, Run 5A1 of the Minnesota experiment.

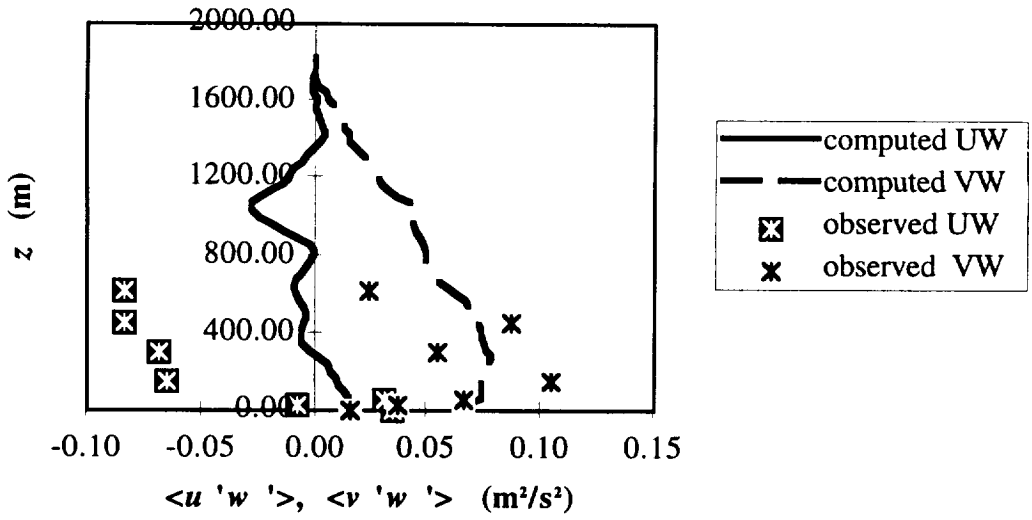

Figure 8. Same as figure 7, but for vertical momentum fluxes.

Figure 9 shows horizontal and vertical velocity variances. Both show good agreement, though there is less vertical mixing in the observed mixed layer than in the modeled mixed layer. This is consistent with the unusually high shear observed in figure 7. It is normally expected that the maximum of the vertical velocity variance should occur at between 1/3 and 1/2 of the inversion height, as shown by the model results. The maximum in the observations, however, is much lower. This same effect can be seen in the heat flux profiles of figure 10. Here, the model shows excellent agreement low in the boundary layer. The observed mixed layer, however, shows an unusually small amount of heat flux. The modeled profile is more what one would expect given the surface heat flux and the inversion height.

Thus, the Minnesota Simulation has shown TASS to be acceptable in predicting turbulent fluxes and variances within the convective atmospheric boundary layer. There seems, however, to have been some mesoscale forcing which caused lower mixing strengths than would be expected for a boundary layer with the given surface heat flux and depth. This effect could not be duplicated because the forcing was not resolved by the synoptic network used to obtain geostrophic wind profiles. In addition, some of the disagreement could be due to the lack of information of the surface heat flux *as a function of time*. Only an average was given for the experimental observation period. In the model, the surface heat flux time dependency was determined such that: (1) roughly the right amount of heat would be added from initialization to middle of the observation period to give the right values of potential temperature, (2) the average surface heat flux for the observation period would have the correct value, and (3) the time dependency would be consistent with diurnal variation. Other small time scale variations, however, could have had an effect.

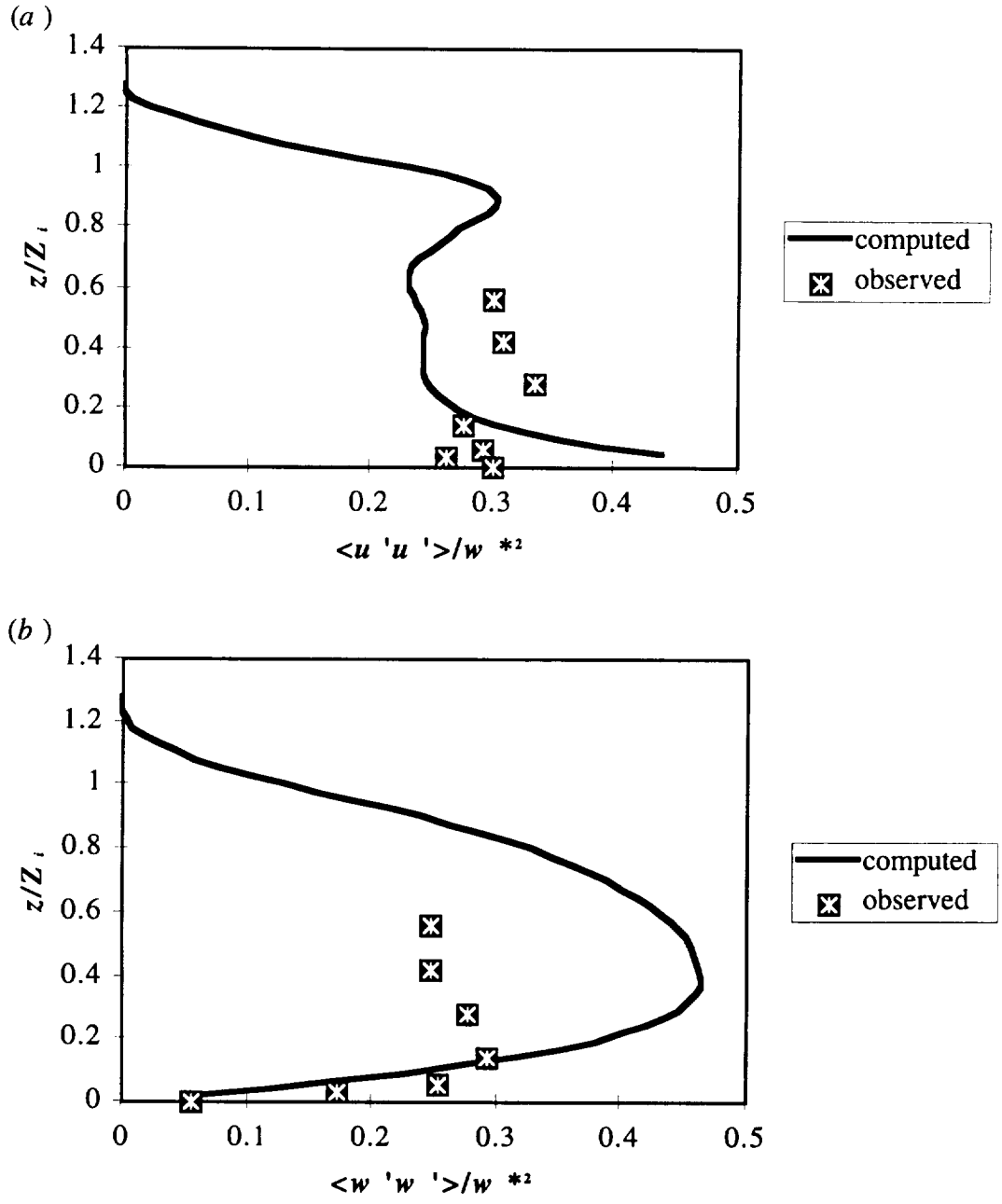

Figure 9. (a) Horizontal and (b) vertical velocity variances for the Minnesota Experiment, Run 5A1.

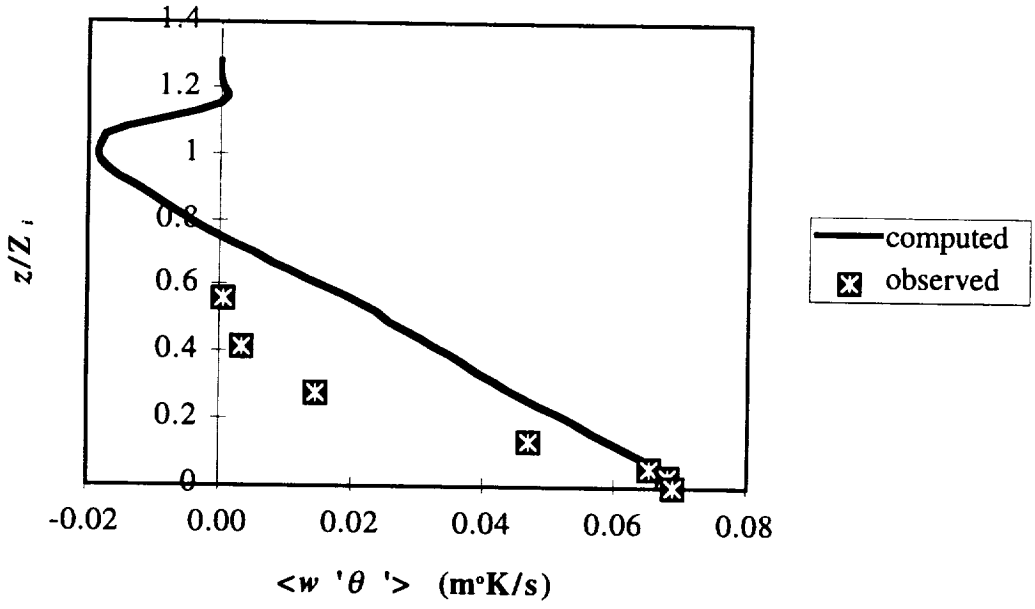

Figure 10. Vertical heat flux for Run 5A1 of the Minnesota Experiment.

4. Neutral boundary layer

Although there are few high quality observational data sets of the overall structure of the neutral atmospheric boundary layer, we can compare with theory and empirical surface layer data (the surface layer is the lowest portion of the boundary layer). Given the postulate that stress is constant within the surface layer, it is found that the dimensionless wind shear, Φ_M is equal to one. This wind shear is expressed as

$$\Phi_M = \frac{kz}{u_*}\sqrt{\left(\frac{\partial\langle u\rangle}{\partial z}\right)^2 + \left(\frac{\partial\langle v\rangle}{\partial z}\right)^2}$$

where u_* is the friction velocity, and k is von Karmann's constant which has been empirically determined to be about 0.4. The friction velocity is expressed as

$$u_* = \tau_0 / \rho$$

where τ_0 is the surface stress. In addition, the dimensionless scalar gradient, Φ_C should be one. This is expressed as

$$\Phi_c = \frac{kz}{c_*} \frac{\partial \langle c \rangle}{\partial z}$$

where $-u_* c_*$ is the surface flux of the scalar c. In order to compare to other computer codes, we have duplicated neutral simulations performed by Andren *et al.* (1994), who compared four computer codes.

Figure 11 shows profiles of Φ_M from *Andren et al.* and from TASS output. We see that, although there is excessive shear close to the ground, TASS shows approximately the same results as most of those in Andren *et al.* The best results for Φ_M are from Mason's code, which employed the backscatter method discussed in Mason and Thomson (1992). The thrust of this technique involves adding random velocities to the calculated velocities close to the ground at each time step. The rationale is that the turbulent eddies there are under-resolved and that this "backscatter" of energy from small scales to large scales will account for the lack of resolution. There are, however, a number of tunable constants in this process and we believe that, for simulating vortices especially, this type of method may lead to more problems than it solves.

Figure 12 shows a comparison of Φ_C between Andren *et al.* and TASS. Here, all values are quite close to one throughout the boundary layer.

(*a*)

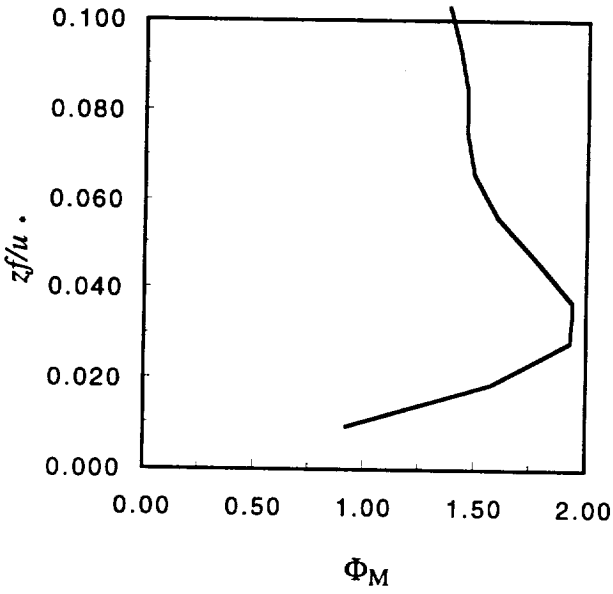

(*b*)

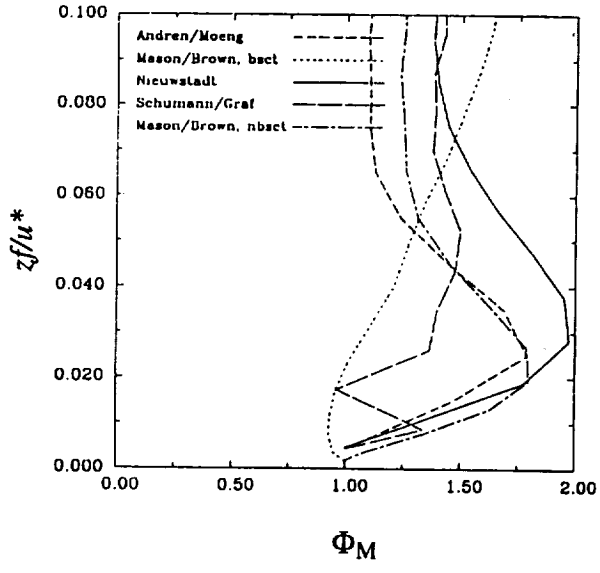

Figure 11. Dimensionless wind shear profiles for a neutral boundary layer from (*a*) TASS and (*b*) Andren *et al.* (1994).

(*a*)

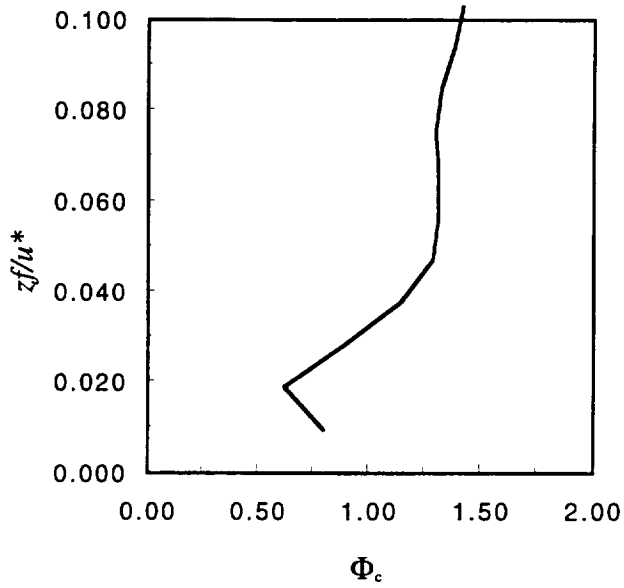

(*b*)

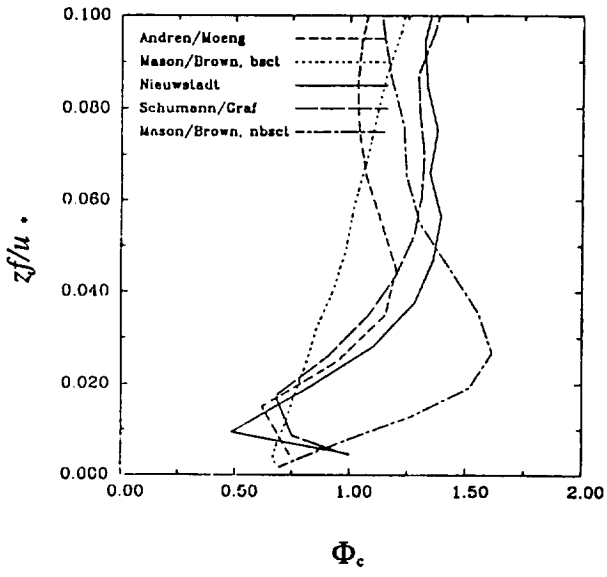

Figure 12. Same as figure 11 but for Φ_C.

5. Summary

In summary, we have added planetary boundary layer simulation capability to TASS and validated results with observed data. There are several options for the surface boundary conditions, one of which is a validated surface energy budget using the slab model. We have made comparisons with both the Wangara and Minnesota boundary layer experiments and have shown that results compare well with the observed data, especially considering the limitations in determining initial conditions.

References

Andren, A. Brown, A. R., Graf, J., Mason, P. J, Moeng, C.-H., Nieuwstadt, F.T.M., & Schumann, U. 1994. Large-eddy simulation of a neutrally stratified boundary layer: A comparison of four computer codes. *Q. J. R. Meteor. Soc.*, **120**, 1457-1484.

Bhumralkar, C. M. 1975. Numerical experiments on the computation of ground surface temperature in an atmospheric general circulation model. *J. Appl. Meteorol.* **14**, 1246-1258.

Blackadar, A. K. 1976. Modeling the nocturnal boundary layer, *Proceedings of the Third Symposium on Atmospheric Turbulence, Diffusion and Air Quality*, pp. 46-49, American Meteorological Society, Boston, MA.

Clarke, R. H., Dyer, A. J., Brook, R. R., Reid, D. G., & Troup, A. J. 1971. The Wangara Experiment: Boundary Layer Data. CSIRO Div. of Meteorol. Phys. Tech. Paper No. 19.

Deardorff, J. W. 1978. Efficient prediction of ground surface temperature and moisture, with inclusion of a layer of vegetation. *J. Geophys. Res.* **83** (C4), 1889-1903.

Izumi, Y. & Caughey, S. J. 1976. Minnesota 1973 Boundary Layer Data Report. Environmental Research Paper No. 547, AFGL, Bedford, MA.

Lettau, H. H. & Davidson, B. 1957. Exploring the Atmosphere's First Mile, vols. 1 and 2. Pergamon, New York.

Lin, Y.-L., Arya, S. P. Kaplan, M. L., & Schowalter, D. G. 1994. Numerical modeling studies of wake vortex transport and evolution within the planetary boundary layer. FY94 Annual Report. Grant #NCC-1-188.

Mason, P.J. & Thomson, D.J. 1992. Stochastic backscatter in large-eddy simulation of boundary layers. *J. Fluid Mech.*, **242**, 51-78.

Pleim, J. E. & Xiu, A. 1995. Development and testing of a surface flux and planetary boundary layer model for application in mesoscale models. *J. App. Met.* **34**, pp. 16-32.

Sellers, W. A. 1965. Physical Climatology. University of Chicago Press, Chicago, Illinois.

Staley, D. O. & Jurica, G. M. 1972. Effective atmospheric emissivity under clear skies. *J. Appl. Meteorol.* **11**, 349-356.

Stull , R. B. 1988. An Introduction to Boundary Layer Meteorology. Kluwer Academic Publishers, Dordrecht.

Zilitinkevich, S. S. 1970. Dynamics of the Atmospheric Boundary Layer, Hydrometeorological Publishing House, Leningrad.

Appendix : Directions for using TASS PBL boundary conditions

To run TASS in the boundary layer mode, one additional input file is needed, fortran unit 7. If this file is not present, the model will run in the original mode In the boundary layer mode, unit 7 must be present for all restarts, and unit 7 must contain the following information.

1. Five logical variable values, format (5L4) each in the following order: UNHEAT, TSPEC, FLXSPEC, EBUDG, TKE. UNHEAT refers to uniform heating. If this variable is true, then a uniform heating is input at the first grid level. The Obukhov length is not explicitly calculated. TSPEC refers to temperature specification. When true, the heat and moisture fluxes are calculated by assuming surface layer similarity. The Obukhov length is explicitly calculated for stress determination. If FLXSPEC is true, then the heat and moisture fluxes are specified in kinematic units. Again, the Obukhov length is explicitly calculated. When EBUDG is true, the energy balance scheme is used to calculate the fluxes. Only one of the previous four variables may be true, otherwise an error message will appear and the run will be terminated. In addition, if any of the above variables are true, a random temperature perturbation is introduced into the first three layers of the domain to start up perturbations on a resolvable scale. When TKE is true, the amount of turbulent kinetic energy at each level in z may be specified.

2. XITMAX, the number of data items for heating specification.

3. Heating data. Each line is free format, with the data in the following order:

if UNHEAT=.T.: time in minutes, heat rate in W/m^2, U(m/s) at top boundary, V(m/s) at top boundary.

if TSPEC=.T.: time in minutes, temperature (C) at z_a, humidity (g/g) at z_a, U(m/s) at top boundary, V(m/s) at top boundary.

if FLXSPEC=.T.: time in minutes, heat flux (K·m/s), moisture flux (m/s), U(m/s) at top boundary, V(m/s) at top boundary.

if EBUDG=.T.: time in minutes, middle cloud fraction, high cloud fraction, U(m/s) at top boundary, V(m/s) at top boundary.

4. If TSPEC=.T., then z_a appears on the line below the heating data items.

5. Logical variable value for GFORCE (L4). If this is true, then the geostrophic wind is specified and the logical variable NOSTEADY should be set to true. If GFORCE is false, NOSTEADY may be either true or false.

6. If GFORCE is true, the next line must contain a logical value to be assigned to GWCONST (L4). If GWCONST is true, the geostrophic wind is constant with height and only one value of the eastward and northward components of the geostrophic winds need be specified.

7. If GFORCE is true, next comes a line delimited list of geostrophic wind values, with the eastward component first and the northward component second on each line.

There must be a line for each K value starting at K=2 and ending at K=KS. If GWCONST is true, then only one line is necessary.

8. If TKE =.T., the next lines contain values of turbulent kinetic energy for each K level starting at K=2 and ending at K=KS-2.

9. The logical value of the variable DFLUX. If true, dust is introduced from the ground throughout the simulation and the environmental values throughout the atmosphere are 0.

10. If DFLUX=.T., the real value of DUSTIN, the dust flux at the surface.

11. If EBUDG=.T., a line containing the values of UTC (the time at 0^o longitude at the initialization time of the model), DAY (the day of the year, between 1 and 365), LNGT (the longitude), and TS (the surface temperature at initialization).

12. If EBUDG=.T., a line containing the values of ALB (ground albedo) , LAMS (thermal conductivity of the soil in m^2/s), TM (the substrate temperature in K), WKW (w_k in m^3/m^3), WMAX (w_{max} in m^3/m^3), W2 (w_2 at initialization in m^3/m^3), and WG (w_g in m^3/m^3 at initialization).

13. If EBUDG=.T., line containing the values of CS ($\rho_s c_s$ in $[J \cdot kg]/[K \cdot m^3]$), EMISS (the ground emissivity), D1PRIME (d_1' in m), and D2PRIME (d_2' in m).

We now show two examples of unit 7 files.

EXAMPLE 1

In this example, KS is 13. The energy budget scheme is employed and a resolved scale turbulent kinetic energy is specified at each level, level 2 being the only non-zero value. The heating value items show no middle or high clouds. Eastward winds at the upper boundary vary from 0.5 m/s at the beginning of the simulation to -4.15 m/s at 999 minutes. Northward winds here vary from 1.10 m/s to 1.47 m/s in the same time period. There are 11 heating data items. There is geostrophic wind specification which is a function of height. There is not dust flux at the surface and the soil parameters and other parameters used for the energy budget scheme appear at the bottom.

```
.F. .F. .F. .T. .T.                  # unheat, tspec, flxspec, ebudg,tke
11                                   # xitmax: number of data items for heating
 0.  0.0  0.0  0.5 1.10
 60.  0.0  0.0  0.07 1.96
120.  0.0  0.0   -1.19 2.60
180   0.0  0.0  -2.23 2.55
240.  0.0  0.0  -1.67 1.96           # time in minutes; middle cloud cover;
300.  0.0  0.0  -2.85 2.10           # high cloud cover; u at top boundary (m/s);
360.  0.0  0.0  -3.13 1.89           # v at top boundary (m/s)
420.  0.0  0.0  -3.83 2.07
480.  0.0  0.0  -3.74 1.79
540.  0.0  0.0  -4.15 1.47
999.  0.0  0.0  -4.15 1.47
.T.                                  # gforce
.F.                                  # gwconst
 -5.4275   0.0
```

```
-5.2825  0.0                          # geostrophic wind values (u,v) in m/s, K=2,13
-5.1375   0.0
-4.9925  0.0
-4.8475   0.0
-4.7025   0.0
-4.5575   0.0
-4.4125   0.0
-4.2675   0.0
-4.1225   0.0
-3.9775   0.0
-3.8325   0.0
 0.365                                # tke values
 0.0
 0.0
 0.0
 0.0
 0.0
 0.0
 0.0
 0.0
 0.0
 .F.                                                  # dflux
23.34   226. -144.93    282.43                       # utc, day, lngt,ts
0.25  0.5E-06  280.5  0.20  0.25  0.0245  0.002     # alb, lams, tm, wkw, wmax, w2, wg
2.1E+06   0.85  0.10  0.50                          # cs, emiss, d1prime, d2prime
```

EXAMPLE 2

In this example, a neutral boundary layer is being studied. Thus the UNHEAT option is used with the heating rate set to 0. We specify a constant geostrophic wind of 10 m/s in the Eastward direction. We also introduce a dust flux of 0.001g/g·s at the lower boundary. Again, KS=13.

```
.T. .F. .F. .F. .T.          # unheat, tspec, flxspec, ebudg, tke
 2                           # xitmax: number of data items for heating
 0.  0.   10.0  0.0          # 0 heating rate, 10 m/s Eastward wind at top of
10000.  0.   10.0  0.0       # domain.
.T.                          # gforce
.T.                          # gwconst:  geos. wind is constant with ht.
10.0  0.0                    # geostrophic wind
0.365                        # tke values for each vertical level
0.295
0.245
0.205
0.175
0.145
0.120
0.100
0.085
0.070
.T.                          # dflux
0.001                        # dustin
```

REPORT DOCUMENTATION PAGE

Form Approved
OMB No. 0704-0188

1. AGENCY USE ONLY (*Leave blank*)	2. REPORT DATE	3. REPORT TYPE AND DATES COVERED
	April 1996	Contractor Report

4. TITLE AND SUBTITLE

Planetary Boundary Layer Simulation Using TASS

5. FUNDING NUMBERS

NCC1-188

538-04-11-11

6. AUTHOR(S)

David G. Schowalter, David S. DeCroix, Yuh-Lang Lin, S. Pal Arya, and Michael Kaplan

7. PERFORMING ORGANIZATION NAME(S) AND ADDRESS(ES)

Department of Marine, Earth and Atmospheric Sciences
North Carolina State University
Box 8208
Raleigh, NC 27695-8208

8. PERFORMING ORGANIZATION REPORT NUMBER

9. SPONSORING / MONITORING AGENCY NAME(S) AND ADDRESS(ES)

National Aeronautics and Space Administration
Langley Research Center
Hampton, VA 23681-0001

10. SPONSORING / MONITORING AGENCY REPORT NUMBER

NASA CR-198325

11. SUPPLEMENTARY NOTES

Langley Technical Monitor: Fred H. Proctor

12a. DISTRIBUTION / AVAILABILITY STATEMENT

Unclassified-Unlimited
Subject Category 34

12b. DISTRIBUTION CODE

13. ABSTRACT (*Maximum 200 words*)

Boundary conditions to an existing large-eddy simulation model have been changed in order to simulate turbulence in the atmospheric boundary layer. Several options are now available, including the use of a surface energy balance. In addition, we compare convective boundary layer simulations with the Wangara and Minnesota field experiments as well as with other model results. We find excellent agreement of modelled mean profiles of wind and temperature with observations and good agreement for velocity variances. Neutral boundary simulation results are compared with theory and with previously used models. Agreement with theory is reasonable, while agreement with previous models is excellent.

14. SUBJECT TERMS

Large-eddy simulation; Planetary boundary layer; Model boundary conditions; Turbulence; Aircraft wake vortices

15. NUMBER OF PAGES

41

16. PRICE CODE

A03

17. SECURITY CLASSIFICATION OF REPORT	18. SECURITY CLASSIFICATION OF THIS PAGE	19. SECURITY CLASSIFICATION OF ABSTRACT	20. LIMITATION OF ABSTRACT
Unclassified	Unclassified	Unclassified	